Journal of Materials Research and Technology 39 (2025) 3594–3607

Contents lists available at ScienceDirect

Journal of Materials Research and Technology

journal homepage: www.elsevier.com/locate/jmrt

Research on sensitivity of strain rate in ultrasonic elliptical vibration cutting of tungsten alloys

Sen Yin [a,b], Menghao Liu [a], Yingjian Tian [a], Fuchen Li [c], Gan Li [d,*], Renke Kang [e]

[a] School of Mechatronics Engineering, Henan University of Science and Technology, Luoyang, 471003, China
[b] Department of Industrial and Systems Engineering, The Hong Kong Polytechnic University, Kowloon, China
[c] Herbert Wertheim College of Engineering, University of Florida, Gainesville, USA
[d] College of Mechanical and Electronic Engineering, China University of Petroleum, Qingdao, 266580, China
[e] State Key Laboratory of High-Performance Precision Manufacturing, Dalian University of Technology, Dalian, 116024, China

ARTICLE INFO

Keywords:
Ultrasonic elliptical vibration cutting
Tungsten alloys
Strain rate
Sensitivity analysis
Surface integrity

ABSTRACT

Ultrasonic elliptical vibration cutting (UEVC) is represents an effective approach for achieving ultra-precision machining (UPM) of tungsten alloys, yet its underlying mechanisms remain incompletely understood. This study investigates the influence of strain rate effects on the material removal and surface formation of UEVC tungsten alloys. First, the strain-stress curves at varying temperatures are obtained by using Hopkinson bar test to verify the strain rate sensitivity of mechanical properties and fracture mechanisms. Then, the strain rate calculation model of UEVC zone is established basing on the dynamic vibration speed of the tool, and the nonlinear relationship between the strain rate and ultrasonic elliptical vibration parameters and cutting parameters is analyzed. The strain rate increases with the increase of two-phase amplitude and phase difference through FE simulation quantitative analysis, and the phase difference is the most sensitive factor. Finally, cutting experiments show that increasing the phase difference can improve the plastic removal mechanism of tungsten alloys and continuously reduce the surface roughness to 32 nm. Concurrently, the increase of phase difference significantly increases the dislocation density to 3×10^{17} m^{-2}, the depth of the grain refinement layer is increased to 1300 nm, and the grain size is significantly reduced, which collectively exhibits potential performance optimization effects on the ion impact resistance of tungsten alloy components.

1. Introduction

Tungsten alloys are two-phase composite materials fabricated via powder metallurgy, primarily composed of tungsten (85 %–99 %) as the matrix, combined with Ni, Fe, Co, Mo, and other major binding phases. Owing to their exceptional properties, including ultra-high hardness, high density, and outstanding radiation resistance [1,2], they are widely recognized as ideal materials for shielding and protecting high-temperature plasma in nuclear fusion devices [3,4]. However, in nuclear fusion devices, tungsten alloy components are exposed to extreme and hostile operating conditions. These include continuous exposure to high-flux irradiation of deuterium-tritium plasma (10^{22}~10^{24} ions/m^2·s), 14 MeV high-energy neutron bombardment ($\geq 10^{18}$ n/m^2·s), and high heat flux (20 MW/m^2 to GW/m^2). If the contour accuracy and surface roughness of these components are not sufficiently high, the synergistic effects of multiple extreme conditions can cause severe surface damage, ultimately leading to functional failure [5,6]. Consequently, developing ultra-precision machining (UPM) techniques to significantly extend the service life of these components has become an urgent priority.

Tungsten alloys are considered classic difficult-to-machine materials. Their dual-phase structure, consisting of hard-brittle tungsten phases and ductile Ni&Fe phases, leads to significant differences in mechanical properties, posing numerous challenges during UPM. Specifically, in ultra-precision single-point diamond turning, the cutting edges are prone to rapid chemical wear and fragmentation [7]. Conversely, in precision grinding, the soft and ductile nickel-iron phases tend to adhere to the grinding wheel surface, significantly reducing its self-sharpening capability [8]. These challenges severely limit the application of conventional machining processes in precision and UPM domains. To address this issue, energy-assisted machining technologies have emerged as a research focus in recent years. For instance, Deng et al.

* Corresponding author.
E-mail address: ligan_2018@163.com (G. Li).

https://doi.org/10.1016/j.jmrt.2025.10.073
Received 3 July 2025; Received in revised form 30 August 2025; Accepted 8 October 2025
Available online 10 October 2025

employed electrochemical polishing [9], while Liu et al. developed dry turning techniques assisted by electroplasticity [10]. These methods have achieved moderate success in improving surface finish quality. However, due to limitations in machining efficiency and curved surface processing capabilities, they still fail to meet the demands of UPM for complex curved structures of tungsten alloy divertors. Thus, developing more efficient machining technologies remains an critical need. Kang et al. [11–13] pioneered the application of ultrasonic elliptical vibration cutting (UEVC) technique to single-point diamond turning of tungsten alloys. By leveraging its intermittent tool-workpiece separation characteristics, they successfully addressed the challenge of diamond tool wear when cutting the soft and ductile nickel-iron phase, significantly enhancing the machinability of tungsten alloys. This breakthrough not only filled a research gap but also laid important technical foundations for subsequent studies. Building on this achievement, Kang's team conducted a series of in-depth investigations, yielding remarkable advancements. Pan et al. [14] established a surface roughness prediction model in UEVC based on deep learning methodologies and optimized the model through discretization analysis. Experimental validation on tungsten alloys confirmed the model's generalizability, providing valuable insights for the development of intelligent machining processes. Subsequently, Pan et al. [15] utilized Raman spectroscopy to compare the surface elements of diamond tools in UEVC and conventional machining (CS) tungsten alloy, revealing that ultrasonic elliptical vibrations effectively suppress the graphitization reaction between diamond tools and nickel-iron binding phases, thereby significantly reducing chemical wear on the diamond tools. Yin et al. [16] developed a high-frequency, large-amplitude single-excitation UEVC system, significantly increasing the critical cutting speed of tools in UEVC and substantially improving machining efficiency. This advancement has opened up broad prospects for the industrial application of UEVC technology. Next, Yin et al. [17] further proposed a dual-excitation UEVC device with controllable elliptical vibration trajectories. By analyzing the amplitude decomposition of elliptical vibration trajectories on different cutting planes, they successfully achieved UPM of tungsten alloy hemispherical components with surface roughness less than 50 nm. Wang et al. [18] employed molecular dynamics simulation techniques to deeply investigate the formation and evolution of microstructures in UEVC tungsten alloys. Their research revealed that the machining force and heat during UEVC were significantly reduced, while the shear stress was notably increased. The elevated shear stress was identified as the primary factor responsible for the increased dislocation density on the machined surface. Additionally, the research team observed a remarkable microstructural evolution on the machined surface under ultrasonic loading, transitioning from sub-grains to ultrafine grains. Zhao et al. [19] combined FE cutting simulations with cutting experiments to systematically investigate the effects of ultrasonic vibrations in different directions on cutting forces and heat generation in tungsten alloys. Through comparative analysis of chip shapes, they elucidated the mechanisms by which UEVC influences the plastic material removal of tungsten alloys. Furthermore, Pan et al. [20] extended their research to the evolution of surface topography and microstructural changes during UEVC of tungsten alloys. By coupling physically based dislocation dynamics models with FE analysis models, they demonstrated how machining parameters such as cutting depth, feed rate, and ultrasonic vibration amplitude and frequency influence surface topography and dislocation density distribution characteristics. In summary, research into UEVC technology for tungsten alloys, including advancements in machining equipment, processes, and surface topography formation mechanisms, has validated the significant advantages of UEVC in UPM (compared to its applications in other difficult-to-machine materials). However, due to the complexity of factors involved, clearly elucidating its mechanisms remains a significant challenge.

It is noteworthy that in UEVC, the integration of ultrasonic vibration with the nominal cutting velocity induces substantial tool acceleration and vibration velocities, thereby significantly elevating the strain rate within the cutting region [21]. The strain rate effect in UEVC has gained considerable attention in recent scholarship due to its substantial implications for material mechanical properties, chip removal mechanisms, and microstructural evolution. Recent research by Wang et al. [22] has examined the interrelations and mechanisms between ultrasonic amplitude, stress field dynamics, microstructural characteristics, and corrosion resistance during the UEAC of pure copper. Their findings indicate a progressive increase in equivalent strain and strain rate with rising ultrasonic amplitudes, accompanied by enhanced grain refinement and thickening of the surface nanocrystalline layer. Building on this, Wang et al. [23] conducted comparative FE simulations and experimental studies to assess variations in physical and microstructural parameters, such as equivalent strain, strain rate, and cutting temperature across UEAC, conventional machining, and traditional extrusion cutting of pure copper. Their results demonstrate that elevated ultrasonic amplitudes substantially raise the equivalent strain rate, with grain sizes transitioning from tens of micrometers to ultrafine levels, underscoring the profound influence of ultrasonic vibration on material behavior under machining. Meanwhile, studies have indicated that tungsten alloy is a strain-rate sensitive material [24], Zhang et al. [25] further demonstrated that an increase in strain rate can lead tungsten alloy to undergo a thermal softening phase, significantly enhancing its plasticity, accompanied by phenomena such as grain refinement and increased dislocation density. Certainly, there are already some preliminary studies available for reference. Bai et al. [26] conducted UEVC tests and observed, through TEM and EBSD, that a continuous ultrafine grain layer microstructure was formed on tungsten alloy surface. They also established a dislocation density evolution model. Their research revealed that the ductile removal mode of tungsten alloys and grain recrystallization phenomena are caused by the high strain rate effects induced by the energy accumulation and dislocation aggregation on the surface due to the ultrasonic elliptical vibration and diamond tool. This discovery raised further questions: during UEVC, the tool, in addition to the nominal cutting speed, is subject to ultrasonic vibration, resulting in high instantaneous acceleration and vibration speed, significantly increasing the strain rate in cutting zone. However, this study primarily unilaterally focuses on the influence of strain rate on the microstructural evolution of tungsten alloys. Yin et al. [27] adjusted the phase difference and combination of ultrasonic vibrations to compare and analyze the generation mechanism of ductile surfaces in tungsten alloy UEVC and explored the role of strain rate in this process. However, this study was primarily limited to a "phenomenological" analysis of surface roughness and hardness, without delving into the mechanisms of microstructural evolution. In summary, the strain rate enhancement induced by UEVC significantly alters the material removal mode of tungsten alloys, thereby profoundly impacting the surface quality and microstructural organization. This, in turn, leads to significant improvements in the assembly precision and service life of tungsten alloy components in nuclear fusion devices.

However, it is noteworthy that the most direct and effective method to achieve high strain rate in machining is by increasing the nominal cutting speed, as demonstrated in the high-speed grinding research conducted by Gao et al. [28]. However, this approach is not suitable for UEVC tungsten alloys. UEVC technology introduces the intermittent cutting characteristic of tool-workpiece separation, preventing the graphitization reaction between the black metal elements in tungsten alloys and diamond tools, which is fundamental to achieving ultra-precision turning of tungsten alloys. Nonetheless, increasing the nominal cutting speed in UEVC would reduce the tool-workpiece separation rate, leading to rapid chemical wear of the diamond tools. Therefore, the nominal cutting speed should be limited to less than one-tenth of the tool vibration speed [29]. Based on this, there is an urgent need to further optimize the strain rate in UEVC tungsten alloys through other effective means. However, systematic research in this area is currently lacking, which not only hinders the continued advancement

of ultra-precision turning of tungsten alloys but also poses an obstacle to explaining the material removal mechanisms of UEVC in other difficult-to-machine metals. Therefore, the unique contribution of this study lies in its advancement beyond previous research concerning the force-heat target in UEVC. Building upon the verification of strain rate sensitivity of tungsten alloys, this research employs FE simulation to circumvent the challenge of direct strain rate measurement during UEVC. It further elucidates the governing principles and sensitivity of ultrasonic elliptical vibration parameters on strain rate within the cutting zone. Departing from conventional process optimization strategies, a novel UEVC optimization strategy for tungsten alloys focused on achieving high strain rates through cutting angle modulation is proposed. This approach not only enables more efficient enhancement of machined surface quality of tungsten alloys but also provides a definitive research direction for the development of specialized UEVC equipment. Additionally, it offers valuable insights and methodologies applicable to the regulation and control of UPM processes for other difficult-to-cut materials.

2. SHPB test for tungsten alloys

To investigate the variations in dynamic mechanical properties of tungsten alloys under different strain rates, Split Hopkinson Pressure Bar (SHPB) tests were employed to gain the dynamic strain-stress curves of tungsten alloys and assess their mechanical performance at elevated strain rates [30].

Fig. 1 illustrates the Schematic and experimental system of SHPB. The SHPB system comprises a driving unit, an incident bar, a specimen, a transmission bar, an absorbing bar, a heating device, and a data acquisition system. Both the incident and transmission bars feature a diameter of 14.5 mm. The specimen utilized in this study is a cylindrical sample measuring 4 mm in diameter and 3 mm in length. Assuming the end face in contact with the incident bar is surface 1, and the end face in contact with the transmission bar is surface 2, during the impact loading process, the displacements of contact surfaces 1 and 2 are u_1 and u_2, respectively. According to the principle of linear superposition of one-dimensional waves, there is:

$$u_1 = \int_0^t c\varepsilon_1 dt = c\int_0^t (\varepsilon_i - \varepsilon_r)dt \tag{1}$$

$$u_2 = \int_0^t c\varepsilon_2 dt = c\int_0^t \varepsilon_t dt \tag{2}$$

Where c is the velocity of the elastic wave in the compression bar, ε_i, ε_r, ε_t are the incident strain, reflected strain, and transmitted strain in the compression bar, respectively. If the initial length and cross-sectional area of the sample are l and A_0, respectively, then the average strain in sample is:

$$\varepsilon_0 = \frac{u_1 - u_2}{l} = \frac{c}{l}\int_0^t (\varepsilon_i - \varepsilon_r - \varepsilon_t)dt \tag{3}$$

The average strain rate of the sample can be obtained by taking the time derivative of Eq. (3):

$$\dot{\varepsilon}_0 = \frac{c}{l}(\varepsilon_i - \varepsilon_r - \varepsilon_t) \tag{4}$$

The end forces acting on sample ends 1 and 2 are respectively:

$$p_1 = EA(\varepsilon_i + \varepsilon_r) \tag{5}$$

$$p_2 = EA\varepsilon_t \tag{6}$$

Where E and A are the elastic modulus and cross-sectional area of compression bar, respectively.

The average value of the force in the sample is:

$$p_m = \frac{p_1 + p_2}{2} = \frac{EA(\varepsilon_i + \varepsilon_r + \varepsilon_t)}{2} \tag{7}$$

The average stress in the sample is:

$$\sigma_0 = \frac{p_m}{A_0} = \frac{EA(\varepsilon_i + \varepsilon_r + \varepsilon_t)}{2A_0} \tag{8}$$

During the loading process, the sample satisfies the dynamic force equilibrium, with $p_1 = p_2$:

$$\varepsilon_i + \varepsilon_r = \varepsilon_t \tag{9}$$

The strain, stress, and strain rate in the sample can be obtained as follows:

$$\varepsilon_0 = -\frac{2c}{l}\int_0^t \varepsilon_r dt \tag{10}$$

$$\sigma_0 = E\frac{A}{A_0}\varepsilon_t \tag{11}$$

$$\dot{\varepsilon}_0 = \frac{2c}{l}\varepsilon_r \tag{12}$$

The strain-stress relationships of tungsten alloys under various strain rates are illustrated in Fig. 2. It is observed that at a constant temperature, as the strain rate increases, the yield strength and flow stress of tungsten alloys rise significantly. This behaviors points to a notable

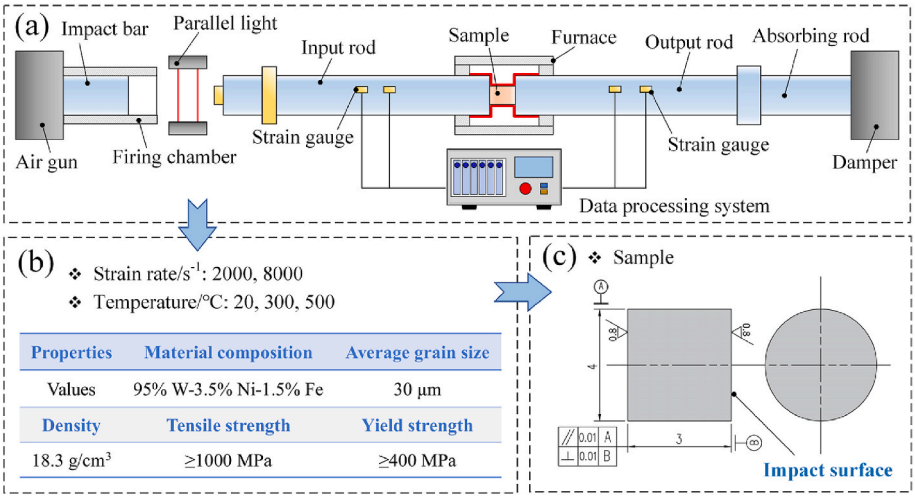

Fig. 1. Schematic and experimental system of SHPB. (a) schematic, (b) mechanical properties of material, (c) system.

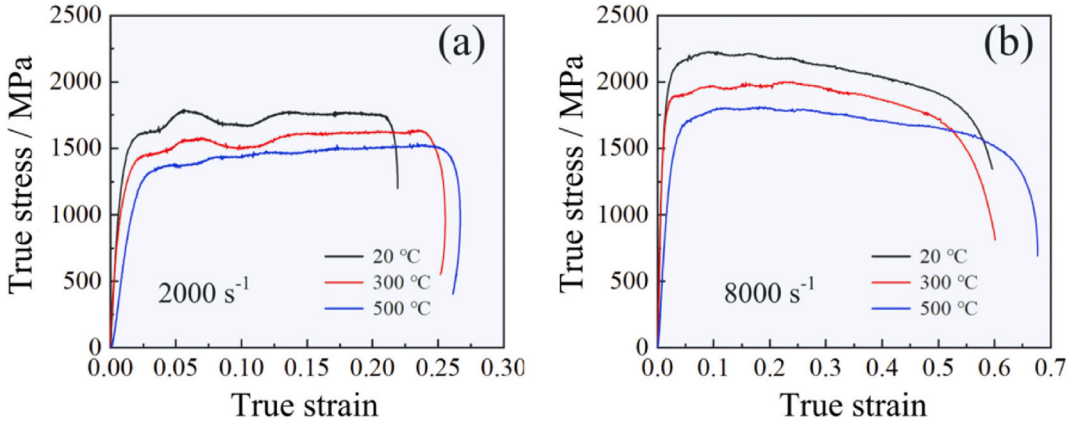

Fig. 2. Strain-stress curves of tungsten alloys at different strain rates. (a) 2000 s^{-1}, (b) 8000 s^{-1}.

strain rate hardening effect, indicating that tungsten alloys are indeed strain rate-sensitive materials. It is noted that SHPB test is not only intended to serve the parameters calibration of Johnson-Cook model, but also to validate the strain rate sensitivity of tungsten alloy materials. Although the strain rate range of SHPB test (10^3~10^4 s^{-1}) lower than that of UEVC (10^5 s^{-1}), research shows that the strain rate sensitivity index of single crystal tungsten remains approximately linear in different strain rate ranges. Therefore, although the mechanical properties of the materials are different under different strain rates, the SHPB test has a certain guiding effect on the cutting process optimization of tungsten alloy materials.

3. Variation of strain rate in UEVC

The empirical formula for the strain rate in machining region during conventional cutting (CC) is expressed as [31,32]:

$$\eta_s = \frac{V_f \cos\gamma_o}{\Delta S_1 \cos(\phi - \gamma_o)} \tag{13}$$

Among these parameters, γ_o represents the nominal geometric rake angle of tool, ΔS_1 denotes the shear slip width, ϕ is the shear angle, and V_f refers to nominal cutting speed.

In context of UEVC, the application of vibrations along two directions significantly enhances the instantaneous impact of the tool on the material within the cutting zone. The exacerbation of mechanical deformation in the machining region induces localised shear displacement of the workpiece material, which subsequently results in a pronounced rise in temperature. The tool vibration speed in UEVC exhibits both magnitude and direction variations throughout a single vibration cycle, as mathematically described in Eq. (14). Specifically:

$$\begin{cases} V_X(t) = 2\pi f A_X \cos(2\pi f t) - V_f \\ V_Y(t) = 2\pi f A_Y \cos(2\pi f t + \Delta\varphi) \end{cases} \tag{14}$$

Among them, Vx is the amplitude in along cutting speed direction, V_Y is the amplitude along cutting depth direction, f is the frequency, $\Delta\varphi$ is the phase difference between two ultrasonic vibrations.

Therefore, the instantaneous relative velocity between the workpiece and tool in UEVC within single vibration cycle can be expressed as:

$$V_1(t) = \sqrt{V_X^2(t) + V_Y^2(t)} \tag{15}$$

Combining Eq. (14) and Eq. (15) can be changed to:

$$V_1(t) = \sqrt{4\pi^2 f^2 A_X^2 \cos^2(2\pi f) + V_f^2 - 2\pi V_f f A_X \cos(2\pi f t) + 4\pi^2 f^2 A_Y^2 \cos^2(2\pi f t + \Delta\varphi)} \tag{16}$$

Additionally, unlike the constant tool rake angle in CC, the actual cutting rake angle of the tool undergoes continuous, instantaneous changes over time throughout each vibration cycle in UEVC. Within a single vibration cycle, the actual cutting rake angle of the tool can be mathematically defined as:

This dynamic variation in the rake angle is a unique characteristic of UEVC, differing significantly from the static tool geometry observed in CC processes.

$$\gamma_o(t) = \begin{cases} \gamma_o + \left|\arctan\dfrac{-2\pi f A_X \sin(2\pi f t) - V_f}{2\pi f A_Y \sin(2\pi f t + \Delta\varphi)}\right| & t_b + n\mathrm{T} \le t < t_m + n\mathrm{T} \\ \gamma_o \quad t = t_m + n\mathrm{T} & \\ \gamma_o - \left|\arctan\dfrac{-2\pi f A_X \sin(2\pi f t) - V_f}{2\pi f A_Y \sin(2\pi f t + \Delta\varphi)}\right| & t_m + n\mathrm{T} \le t < t_e + n\mathrm{T} \end{cases} \tag{17}$$

Among them, γ_o(t) is the actual cutting front angle, t_m is the lowest point of locus in UEVC, t_b is the starting moment of UEVC for a vibration cycle, t_e is the end moment of UEVC for a vibration cycle.

Additionally, the material removal process in UEVC is illustrated in Fig. 3(a). The diamond tool initiates material cutting at position K_1 and completes the cutting cycle at position K_3, with K_2 representing the endpoint of the previous cutting cycle. Consequently, within a single vibration cycle of UEVC, the material removal volume corresponds to the region enclosed by K_1–K_2–K_3. In both CC and UEVC, the parameter a_e can be regarded as the nominal cutting depth. However, in UEVC, the elliptical cutting locus results in a continuously varying cutting depth as the cutting position changes, with l_{ch} denoting the maximum cutting thickness. Compared to the constant material removal rate in CC, the material removal amount in a single UEVC vibration cycle is time-dependent and significantly smaller. This dynamic nature of material removal leads to the shear slip width (ΔS_1) being a time-varying parameter within a single vibration cycle.

Based on the tool's motion trajectory in UEVC, a shear angle model is established, as depicted in Fig. 3(c). At a specific cutting position, the frictional force on the tool rake face is denoted as F_f, and the combined force is represented as F_s. The shear force on the shear plane is F_r. As shown in Fig. 3(d), the relationship between the shear force (F_r) and the cutting force (F_s) of the shear plane can be expressed as:

$$F_r = F_s \cos(\phi + \beta - \gamma_o) = \tau_s A_s = \tau_s A_c / \sin\phi \tag{18}$$

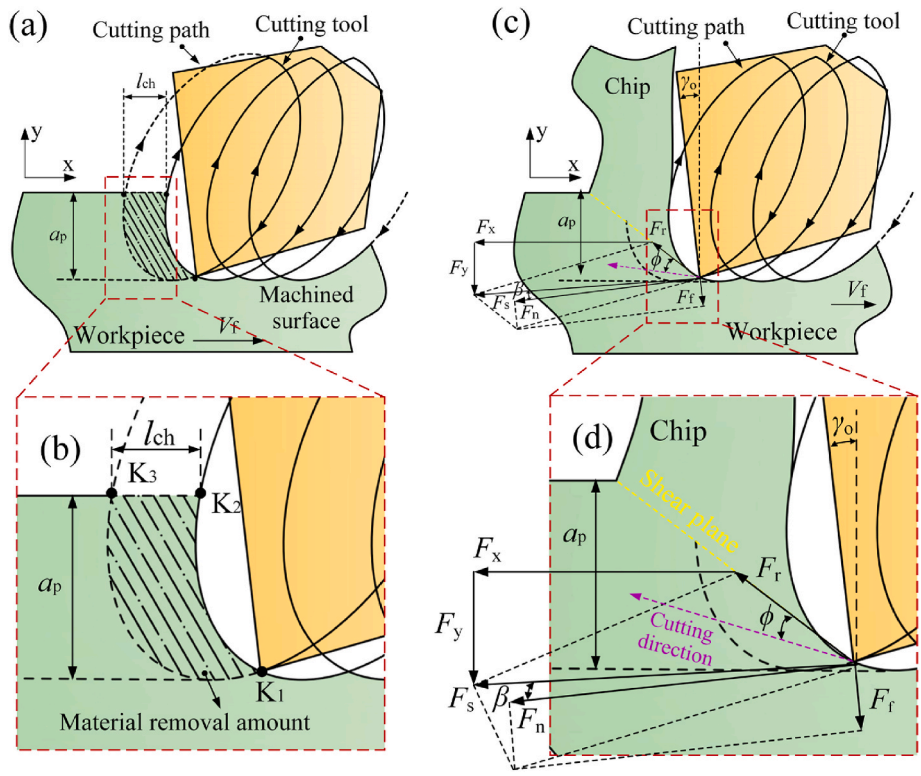

Fig. 3. Material removal and shear angle calculation model in UEVC. (a) Material removal amount, (b) partial enlargement, (c) Shear angle, (d) partial enlargement.

$$F_s = \tau_s A_c / \cos(\phi + \beta - \gamma_o)\sin\phi \tag{19}$$

Among them, ϕ is shear angle, β is average friction angle between the tool rake face and chips, γ_o is the actual rake angle of tool, τ_s is the nominal shear strength of the workpiece material, A_s is the shear plane area, A_c is the cutting cross-sectional area. However, it is worth noting that in UEVC, A_s and A_c are time-varying within a single vibration cycle, which are related to ultrasonic vibration parameters and cutting parameters, making quantitative analysis impossible. However, this does not affect the qualitative research of this study on the influencing factors of strain rate in the cutting zone.

Therefore, the component force F_z along Z direction is:

$$F_x = F_r\cos(\beta - \gamma_0) = \frac{\tau_s A_c}{\sin\phi}\cdot\frac{\cos(\beta - \gamma_0)}{\cos(\phi + \beta - \gamma_0)} \tag{20}$$

In CC, the cutting component force F_x is differentiated with respect to the shear angle and set equal to 0 to obtain the shear angle ϕ, as shown in Eq. (21). Furthermore, the shear angle models proposed by Merchant [33] and Lee and Shaffer [34], as shown in Eq. (22), are widely used.

$$2\phi + \beta - \gamma_0 = \pi/2 \tag{21}$$

$$\phi + \beta - \gamma_0 = \pi/4 \tag{22}$$

However, these methods are not applicable for calculating the shear angle in UEVC.

Analyzing the reasons for this limitation, in CC, the tool acceleration is zero, the rake angle remains constant, and the average friction angle between the chip and the tool rake face is relatively stable throughout the cutting process. Additionally, the cutting cross-sectional area remains fixed. Conversely, in UEVC, the tool acceleration is non-zero and time-varying, and both the cutting cross-sectional area and the tool rake angle exhibit periodic variations. Consequently, under these conditions, it can only be qualitatively concluded that the shear angle in UEVC is time-varying, while a quantitative analysis cannot be performed.

Therefore, the strain rate in the machining region of UEVC within a single vibration cycle can be expressed as:

$$\eta_s(t) = \frac{V_1(t)\cos[\gamma_o(t)]}{\Delta S_1(t)\cos[\phi(t) - \gamma_o(t)]} \tag{23}$$

Combining the previous formula, the strain rate of the cutting zone in UEVC within a single vibration cycle is:

$$\eta_s(t) = \frac{\sqrt{4\pi^2 f^2 A_X^2\cos^2(2\pi f) + V_f^2 - 2\pi V_f f A_X\cos(2\pi f t) + 4\pi^2 f^2 A_Y^2\cos^2(2\pi f t + \Delta\varphi)}\cos[\gamma_o(t)]}{\Delta S_1(t)\cos[\phi(t) - \gamma_o(t)]} \tag{24}$$

According to Eq. (24), the strain rate $\eta_s(t)$ in UEVC is a time variable that is related to many factors, including nominal cutting speed V_f, the tool geometric rake angle γ_0 and ultrasonic vibration parameters, including the two-phase vibration amplitude A_X and A_Y, and phase difference $\Delta\varphi$ and the vibration frequency f.

In summary, the introduction of ultrasonic elliptical vibration in UEVC induces dynamic, nonlinear variations in critical cutting parameters including tool rake angle, shear slip width, shear angle, and cutting speed. These parameters evolve into time-dependent variables,

complicating the cutting process beyond the capabilities of traditional analytical methods. To address this complexity, FEM is utilized to simulate and analyze the UEVC process effectively. FEM enables researchers to model the intricate interactions and nonlinear behaviors inherent to UEVC, facilitating the optimization of the process for improved machining outcomes. While FEM offers significant insights, its implementation demands substantial computational resources and expertise. Practical considerations, such as the feasibility of implementing UEVC in various industrial settings, the adaptability of existing machinery, and the cost-benefit analysis of its use, are essential areas for further exploration and experimentation.

4. Effect of vibration parameters on strain rate

4.1. FE cutting model

Due to the difficulty in quantitatively analyzing the strain rate in UEVC through theoretical analysis, this study introduces FE simulation to investigate the influence and sensitivity of ultrasonic vibration parameters on the strain rate in the cutting zone. A 2D-FE cutting model was constructed using ABAQUS, excluding material phase transformations and tool elastic deformation effects, as illustrated in Fig. 4. The hard and brittle tungsten phase in the tungsten alloy, combined with the impact generated by ultrasonic vibration, can easily cause fatigue chipping of the diamond tool. Therefore, the diamond tool must have a certain geometric rake angle to ensure rigidity. In the model, the rake and clearance angles of the single-crystal diamond tool were set to 0° and 12°, respectively, with a tool edge radius of 100 nm. The workpiece dimensions were 40 μm in length and 25 μm in width.

To optimize computational efficiency, a differential meshing strategy was adopted for workpiece discretization [35,36], with the minimum element size set to 0.2 μm. Both the tool and workpiece utilize CPE4RT element types, with 326 elements for the tool and 16,800 elements for the workpiece [19]. Fixed constraints were applied to the left sides and bottom of the workpiece. Johnson-Cook constitutive model was employed to simulate the mechanical behavior of tungsten alloys, accounting for strain-stress relationships, strain rate effects, and thermal interactions. This model is particularly accurate in describing the mechanical response of metallic materials under high plastic strain rates. The flow stress calculation formula for tungsten alloys, based on Johnson-Cook model:

Table 1
Johnson-Cook constitutive parameters of tungsten alloys.

Category	A/MPa	B/MPa	C	n	m	T_m/°C	ε_0/s^{-1}
Value	705.66	819	0.3	0.0475	0.813	1900	0.001

$$\overline{\sigma}=\left[1+C\ln\left(\frac{\varepsilon_2}{\varepsilon_1}\right)\right]\left[1-\left(\frac{T-T_r}{T_m-T_r}\right)^m\right][A+B(\varepsilon_3)^n] \tag{25}$$

where ε_2 denotes the equivalent plastic strain rate, ε_1 represents the reference plastic strain rate, ε_3 is the equivalent plastic strain, Tr is the room temperature, Tm represents melting temperature. A denotes reference strain rate and yield strength, B represents the strain hardening coefficient, C is the strain hardening index, n represents the sensitivity index of corresponding strain rate, and m denotes the temperature softening index.

Johnson-Cook failure criterion was also implemented to simulate material failure. Convection heat transfer boundary conditions were applied to model the oil cooling process. Material parameters and failure criteria are detailed in Table 1, respectively.

Table 2
UEVC single-factor simulation experiment parameters.

No.	$\Delta\varphi$	A_x/μm	A_y/μm	f/kHz	V_f/m/min	a_p/μm	Cooling
1	π/2	1	3	25	2	4	Oil
2		2					
3		3					
4		4					
5		5					
6		3	1				
7			2				
8			3				
9			4				
10			5				
11	π/12		3				
12	π/6						
13	π/4						
14	π/3						
15	π/2						

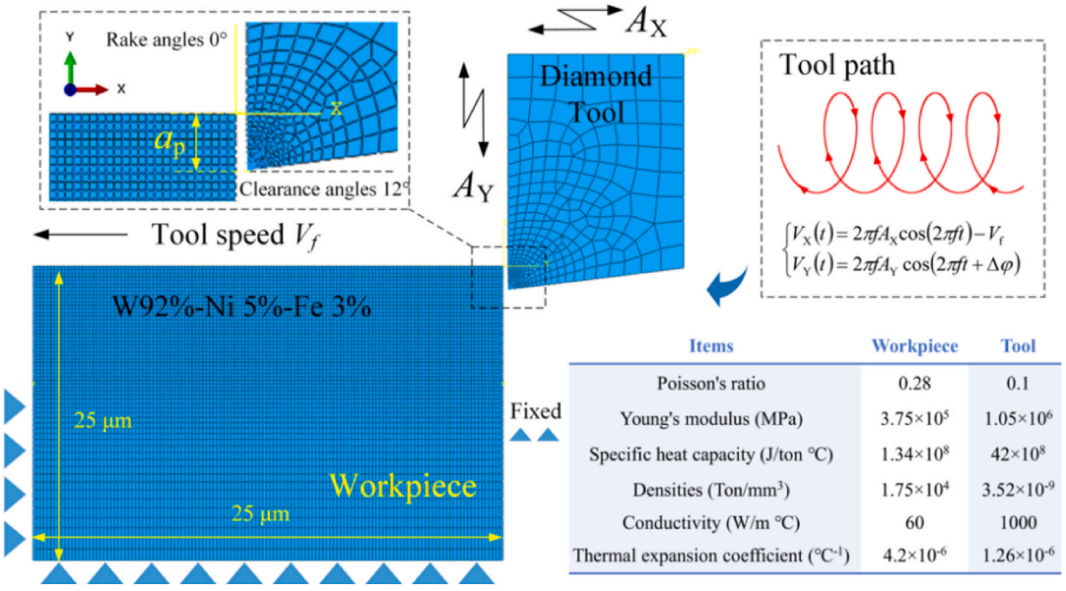

Fig. 4. FE model of UEVC for tungsten alloys.

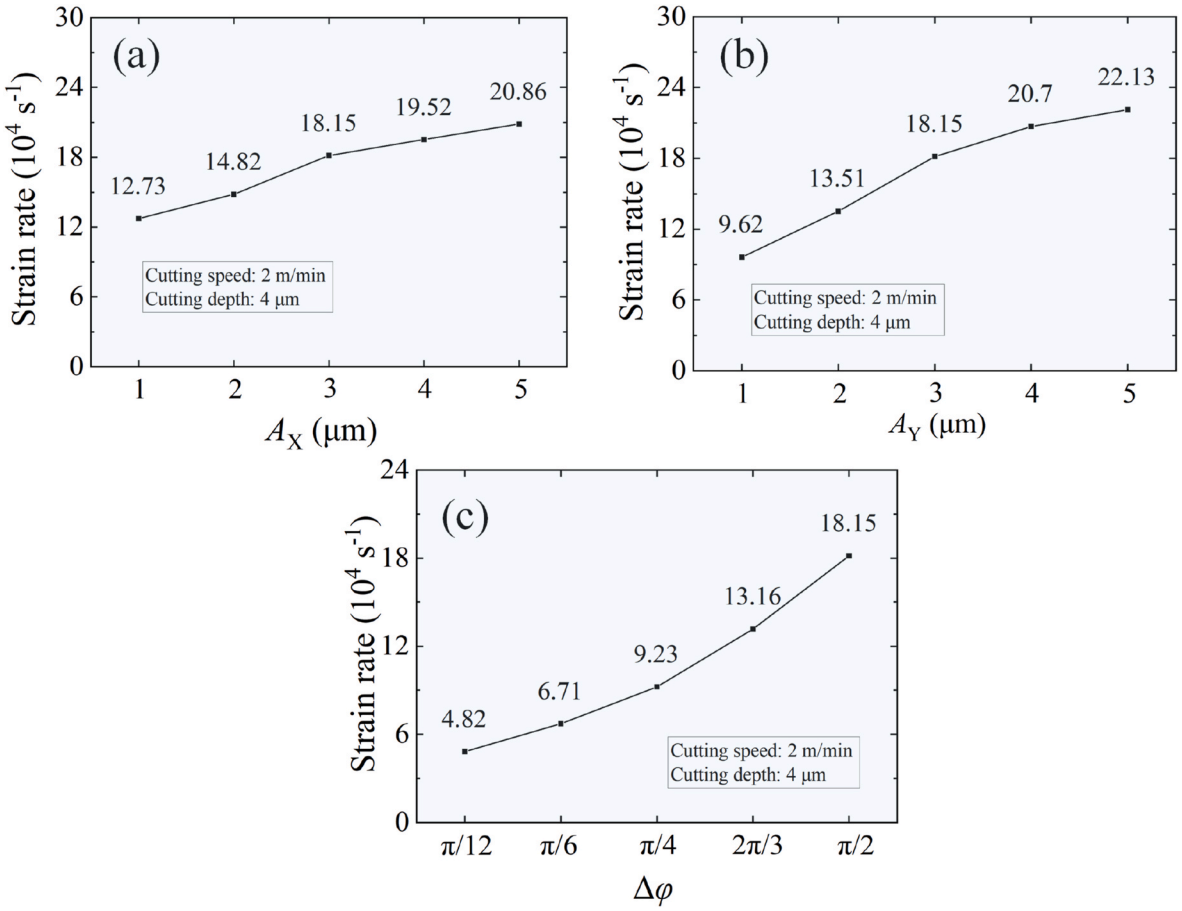

Fig. 5. Influence of vibration parameters on strain rate in cutting zone. (a) A_X, (b) A_Y, (c) Δφ.

4.2. Single-factor cutting simulation

It can be seen from Eq. (24) that the strain rate in cutting zone in UEVC is related to the ultrasonic vibration parameters (two-phase amplitude A_X and A_Y, phase difference $\Delta\varphi$ and frequency f) and the cutting parameters (nominal cutting speed V_f). In order to ensure the separation effect of tool and workpiece, the nominal cutting speed V_f is strictly limited and should not be used as an optimization parameter. Meanwhile, Since UEVC systems are typically based on the resonance principle of the overall mechanical structure, the vibration frequency cannot be adjusted once the structure is determined, making the resonant frequency unsuitable as an optimization parameter [37–39]. Therefore, the variables selected for this study are A_X, A_Y and $\Delta\varphi$.

The simulation experiment parameters are detailed in Table 2. Since the vibration frequency is the same, the peak value of strain rate change in the UEVC path during a single vibration period is extracted. The impact of vibration parameters on strain rates in the UEVC region of tungsten alloys is illustrated in Fig. 5. The results indicate that the strain rate in cutting zone increases with A_X in cutting velocity direction, reaching 2.09×10^5 s^{-1} at $A_X = 5$ μm, as illustrated in Fig. 5(a). Similarly, the strain rate increases with the amplitude A_Y in the cutting depth direction, reaching 2.21×10^5 s^{-1} at $A_Y = 5$ μm, as illustrated in Fig. 5 (b). Consequently, an increase in the two-phase amplitude significantly enhances the vibration speed of the tool, thereby increasing the relative speed between the tool and workpiece. This constitutes the fundamental mechanism by which amplitude elevation augments the strain rate in the cutting zone, which is consistent with the conclusion derived from Eq. (24). Furthermore, the strain rate increases with $\Delta\varphi$ in the range of

Table 3
Orthogonal simulation experiment parameters.

No.	$\Delta\varphi$	A_x/μm	A_y/μm	f/kHz	V_f/m/min	a_p/μm	Cooling	strain rate/s^{-1}
16	π/6	1	1	25	2	4	Oil	34600
17	π/3	1	3					110000
18	π/2	1	5					139400
19	π/2	3	3					181500
20	π/6	3	5					171000
21	π/3	3	1					42200
22	π/3	5	5					143000
23	π/2	5	1					146000
24	π/6	5	3					97800
Average A	74250	94500	101550					
Average B	98500	132000	129600					
Average C	155560	129050	151650					
Variance R_1	81310	37500	50100					

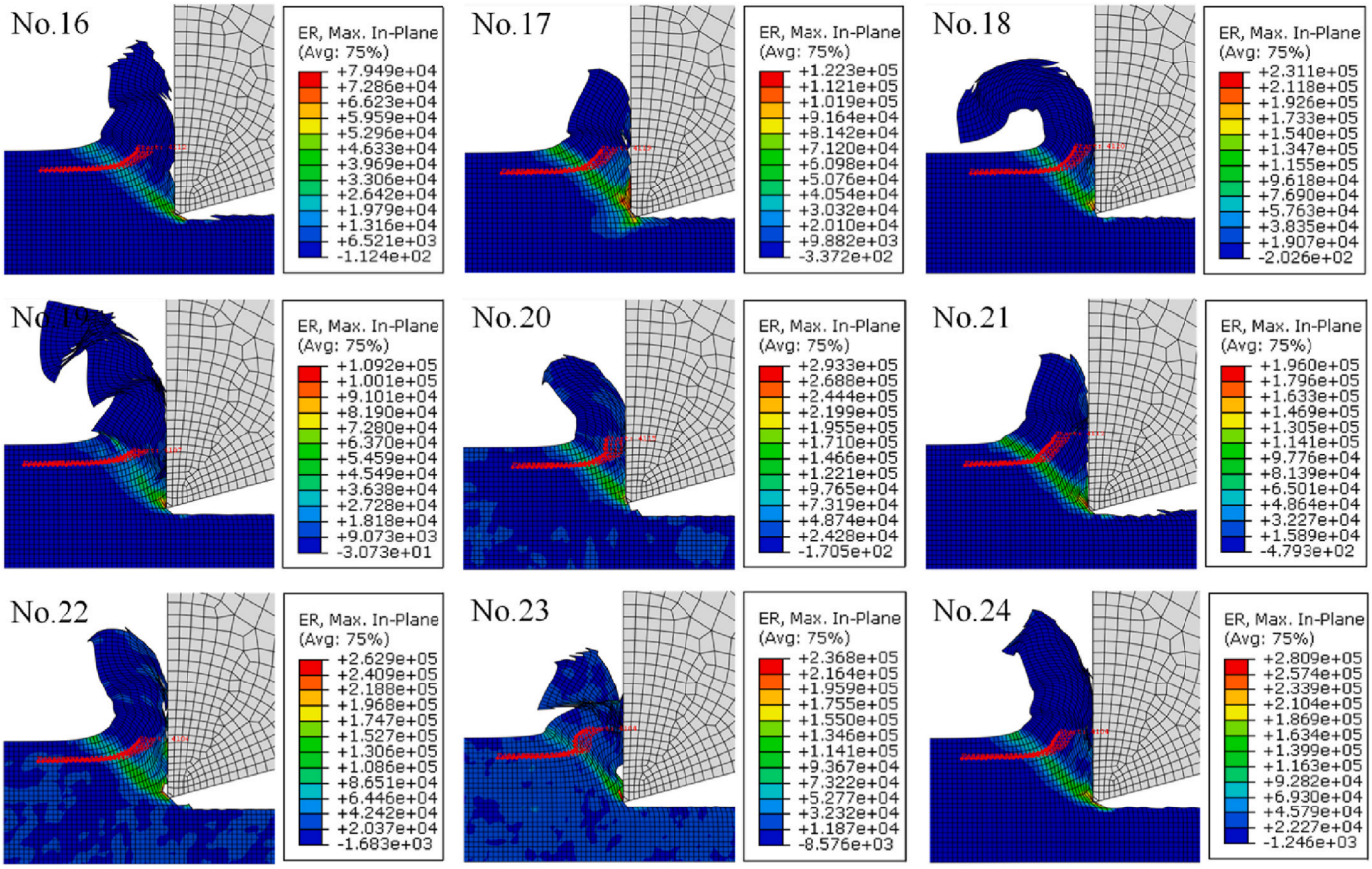

Fig. 6. Influence of vibration parameters on machined surface profile and chip morphology.

0°–90°, as shown in Fig. 5(c). When the phase difference reaches 90°, the strain rate attains 1.81 × 10^5 s^{-1}. This provides the theoretical basis for process optimization. The ultrasonic vibration parameters may be optimized to regulate the strain rate within cutting zone of tungsten alloys, thereby modulating the material removal mechanism and surface formation characteristics to further enhance UEVC quality of tungsten alloys.

4.3. Multifactor orthogonal cutting simulation

To determine the sensitivity of ultrasonic vibration parameters on the strain rate in cutting region, a three-factor, three-level orthogonal cutting simulation experiment was designed. The simulation parameters are detailed in Table 3.

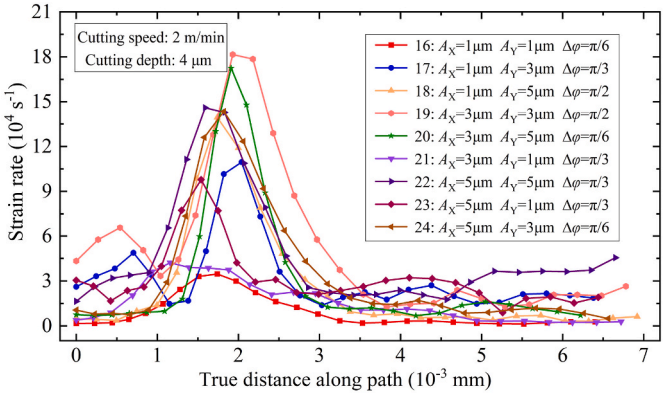

Fig. 7. Effect of vibration parameters on the strain rate along path I of UEVC.

Fig. 6 reveals the mechanisms by which ultrasonic elliptical vibration parameters influence the surface topography and chip morphology of tungsten alloys. Differences in chip morphology indicate that varying combinations of amplitude and phase difference significantly affect the material removal mechanisms in UEVC. Among them, while the strain rate within the cutting zone cannot be quantitatively analyzed, a distinct correlation is observable. Under elevated strain rate conditions (e.g., Experiments No. 18, 19, and 20), continuous chip morphology indicates material removal primarily through plastic deformation mechanisms. This removal mode is conducive to achieving superior surface quality. Conversely, under reduced strain rates (e.g., Experiments No. 16, 21, and 24), frequent chip fracture occurs, signifying a predominantly brittle removal mechanism for the tungsten alloy material. Additionally, variations in the vibration trajectories result in differences in the residual heights on the cutting surfaces, thereby influencing surface roughness to a certain extent.

Fig. 7 illustrates the impact of vibration parameters on the strain rate along Path I during the cutting process of the tungsten alloy. Different combinations of amplitude and phase difference significantly influence the strain rate in the UEVC region. An extremal difference analysis of the strain rate results is presented in Table 3. By analyzing R_1, the primary and secondary factors influencing the strain rate in UEVC region of tungsten alloy can be identified as follows: phase difference, amplitude along cutting depth direction, and amplitude along cutting velocity direction. This provides a critical reference for optimizing the UEVC process for tungsten alloys. The amplitude (A_x and A_y) and phase difference $\Delta\varphi$ of the two-phase vibration serve as key parameters for regulating the strain rate within the cutting zone during UEVC of tungsten alloys, thereby enabling process optimization. However, from a machining perspective, excessively large amplitudes, while increasing the strain rate further, prove detrimental to machining stability,

particularly in UPM applications. Firstly, large amplitudes induce pronounced vibration marks on the machined surface, significantly deteriorating surface roughness. Secondly, large amplitudes intensify tool impact forces, increasing the risk of tool chipping and reducing tool life. Furthermore, given that phase difference exhibits the highest sensitivity in influencing the strain rate within the cutting zone, it was selected as the primary process optimization parameter for UEVC experiments of tungsten alloys.

5. Cutting experiments and the results

5.1. Cutting experiments

In this study, an innovative ultrasonic vibration driving mechanism was developed for UEVC device, with its core ultrasonic vibration unit comprising two sets of piezoelectric ceramic stacks. The dual-channel ultrasonic generator utilizes Direct Digital Synthesis (DDS) to generate a reference sine wave and employs a digital phase shifter (with a resolution of up to 0.1°) for phase control, which features two independent Class D resonant amplifiers and outputs two-phase excitation signals, effectively exciting the longitudinal and bending vibration modes of the ultrasonic vibration unit, achieving longitudinal-bending vibration. By adjusting the phase difference and voltage of the two-phase excitations, the device can generate various ultrasonic elliptical vibration trajectories, meeting different processing requirements.

To evaluate the vibration performance of the self-developed UEVC device, a Doppler laser vibrometer (OFV-505, Polytec GmbH) was employed for testing, as shown in Fig. 8(a). The measured resonant frequency was 25.6 kHz, with an amplitude of 2.2 μm along the cutting speed direction (A_X) and 2.1 μm along the cutting depth direction (A_Y). Additionally, Fig. 8(b)–(d) illustrates the ultrasonic elliptical vibration trajectories under various phase differences.

The cutting tests were conducted on a ZCS-QGM350A ultra-precision lathe (manufactured in China), as shown in Fig. 9. A face-turning method was adopted, with the workpiece measuring 15 mm in diameter and composed of tungsten alloy. The material composition was consistent with that used in the Hopkinson bar experiments described in Chapter 2. A natural diamond tool was used, featuring a rake angle of 0°, a relief angle of 12°, and a cutting edge radius of 1 mm. Detailed experimental parameters are listed in Table 4. Cutting force data were recorded using the Kistler 9109A dynamometer, operating in a measurement range of −500 N–500 N, with a minimum sensitivity of 0.002 N to ensure precise accuracy. For verifying FE models, common methods include cutting force, cutting temperature, and chip morphology; among these, cutting force verification proves the most reliable. However, the voltage stabilization module and current feedback module within the self-developed UEVC device interfered with dynamometer signal acquisition. Therefore, the method of verifying the cutting force in CC was adopted, comparing it with forces measured in CC experiments. Through iterative optimization, the Failure Displacement and Friction Coefficient for the optimized FE model were determined under defined conditions: Failure Displacement set to 0.00065 and Friction Coefficient to 0.2.

5.2. Results of the cutting experiment

The surface topography and roughness were precisely measured using a white light interferometer (Zygo, NV5000 502S), with three different measurement points selected for each workpiece. Fig. 10(a) presents a comparison of the surface roughness of tungsten alloy under different phase difference conditions. The results indicate that the phase difference has a significant impact on the surface roughness. Within a phase difference range of 30°–90°, the surface roughness parameter *Ra* decreases as the phase difference increases. When the phase difference reaches 90°, the smallest surface roughness *Ra* value of 32 nm is achieved in UEVC.

The microscale surface topography of the cutting surfaces under different phase differences was observed using a scanning electron microscope (SEM, USA, FEI, Q45). As illustrated in Fig. 11. The microscopic fracturing on the workpiece surface gradually diminished as the

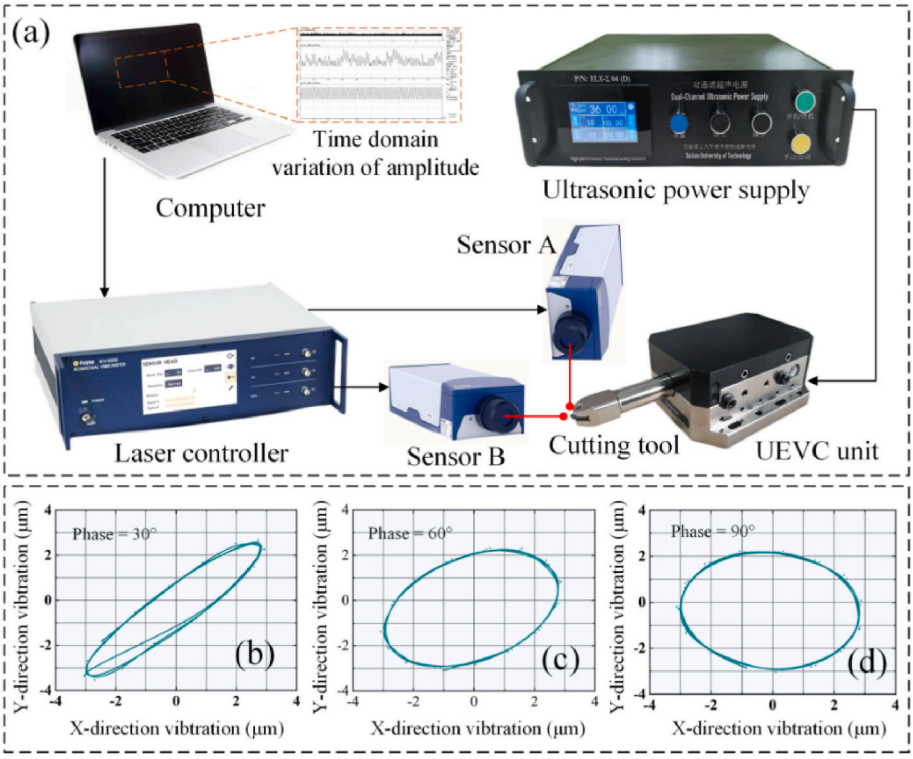

Fig. 8. Principle and results of vibration performance testing for UEVC system. (a) testing principle, (b) vibration trajectory with 30° phase difference, (c) vibration trajectory with 60° phase difference, (d) vibration trajectory with 90° phase difference.

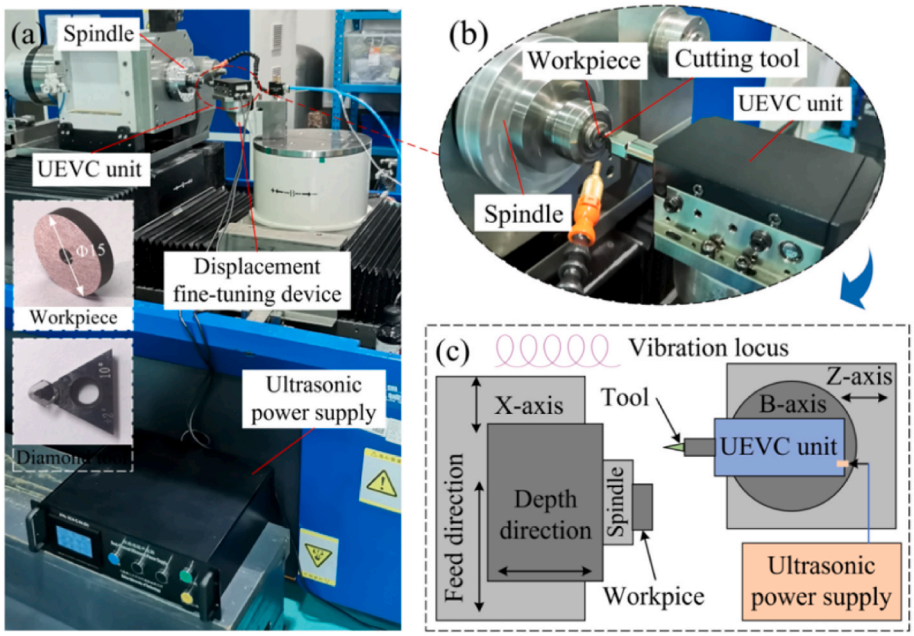

Fig. 9. Experimental principle and site. (a) site, (b) cutting mode, (c) principle.

Table 4
Experimental parameters of UEVC with different phase differences.

No.	$\Delta\varphi$	A_X/ μm	A_Y/ μm	f/ kHz	V_f/m/ min	a_p/ μm	S/μm/ r	Cooling
1	π/6	2.2	2.1	25.1	2	4	20	Oil
2	π/3							
3	π/2							

phase difference increased, with clear vibration marks left by the ultrasonic vibration. When the phase difference reached 90°, as shown in Fig. 11(e) and (f). The cutting surface exhibited minimal fracturing or wrinkling, displaying typical plastic removal characteristics. The underlying reason is that the increase in strain rate not only alters the mechanical properties of the material, but also induces a local temperature rise due to the high strain rate effect, as illustrated in Fig. 10(b). These combined effects enhance the plastic deformation of tungsten alloys. Experimental results demonstrate that the phase difference, as a critical parameter in UEVC, significantly influences the cutting deformation mechanism and microstructural response of tungsten alloys. A comparison of TEM characteristics under 90° and 30° phase differences reveals inherent differences in their internal mechanisms.

Under 90° phase difference conditions, the material removal process is subjected to high strain rates and complex periodic "tensile-compressive" stresses. At a high strain rate in the cutting zone (Refer to Fig. 5(a), reaching 1.8×10^5 s^{-1}), the dislocation nucleation rate is significantly higher than the dynamic recovery rate, resulting in a dislocation density of 3×10^{17} m^{-2} and the formation of dense dislocation tangles and stacking faults, As shown in Fig. 12. The thickness of the grain refinement layer reaches 1300 nm, indicating that severe plastic deformation triggers a continuous dynamic recrystallization (CDRX) process: the initial coarse grains are divided into subgrains by dislocation walls and evolve into nanocrystalline grains under shear stress. High-resolution TEM shows that the atomic spacing is compressed to 0.237 nm (theoretical value: 0.316 nm), suggesting local lattice distortion originating from high-pressure states in shear bands, potentially related to non-uniform deformation due to restricted {110} slip systems in the BCC structure of tungsten. Additionally, the presence of stacking faults suggests low-energy dislocation expansion behavior.

At a 30° phase difference, the non-linear features of the elliptical trajectory are weakened, reducing the cutting strain rate to 10^5 s^{-1}. Under this condition, dislocations undergo dynamic recovery through climb and cross-slip, resulting in a dislocation density (10^{17} m^{-2}) that is 67 % lower than that at 90° phase difference. As shown in Fig. 13, The thickness of the grain refinement layer is only 600 nm, with narrow elongated grain boundaries, indicating that incomplete recrystallization

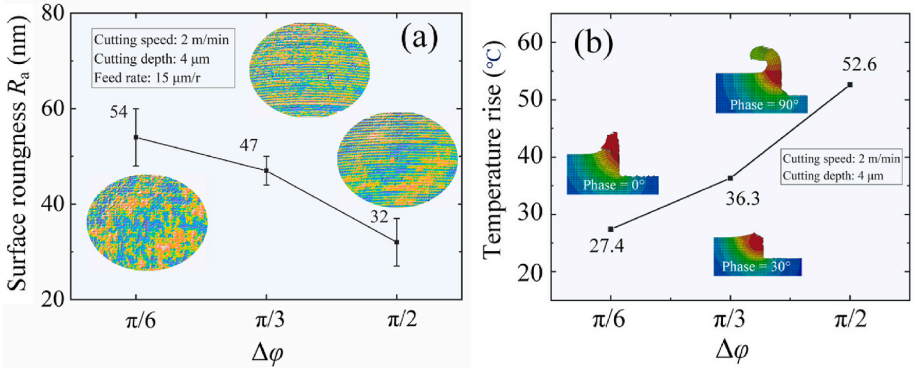

Fig. 10. Surface roughness and temperature rise of tungsten alloys in UEVC with different phase differences. (a) surface roughness in experiments (b) temperature rise in FEM.

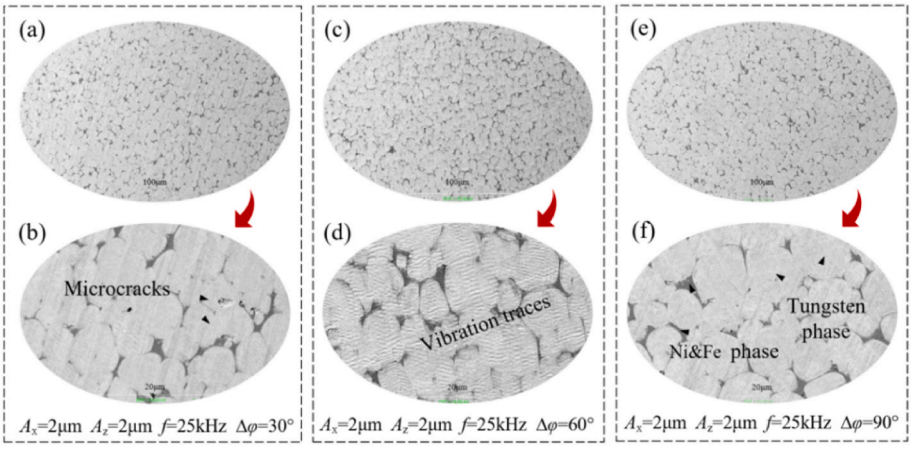

Fig. 11. Surface morphology of tungsten alloys in UEVC with different phase differences. (a) 30°, (b) partial enlargement, (c) 60°, (d) partial enlargement, (e) 90°, (f) partial enlargement.

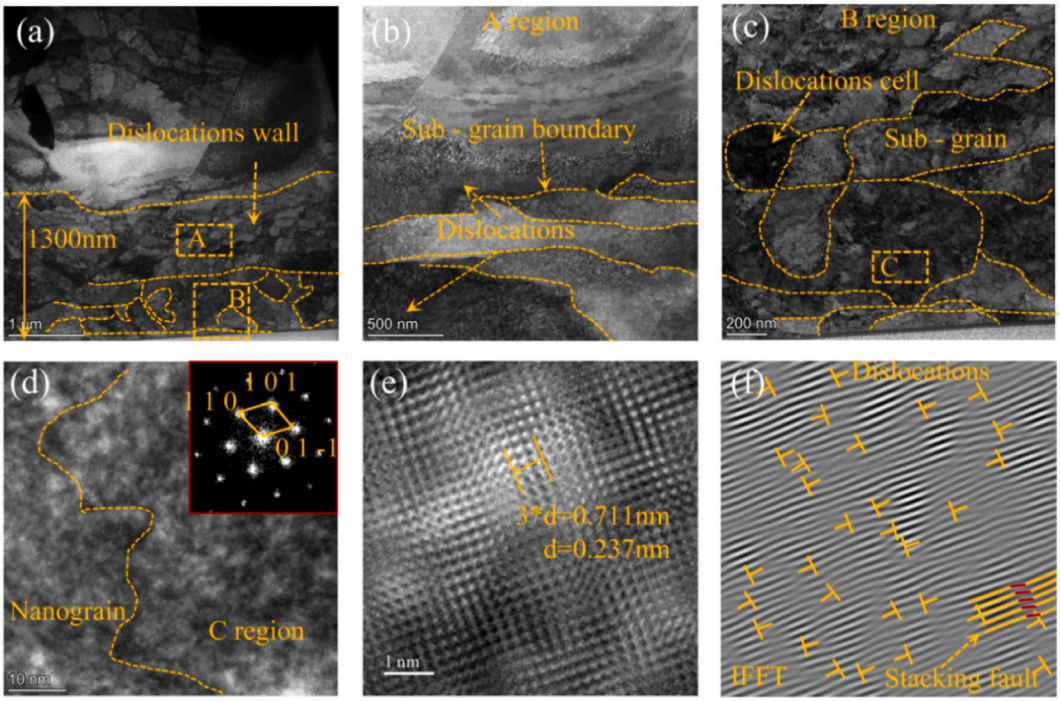

Fig. 12. Microstructural features of tungsten alloys in UEVC with 90°. (a) general view of microstructure gradient variation, (b) nanocrystalline feature of A region, (c) nanocrystalline feature of B region, (d) nanocrystalline feature of C region, (e) interplanar spacing of C region, (f) inverse Fast Fourier Transform (IFFT) of C region.

dominates: deformation energy is released through grain boundary migration rather than grain fragmentation. The atomic spacing returns to 0.308 nm, close to the theoretical lattice constant of tungsten, reflecting stress relaxation effects. The phase difference regulates the strain rate and thermodynamic states in UEVC process, enabling targeted control of the deformation mechanism in tungsten alloys. Compared to the microstructure of phase difference at 90°, apart from the variation in strain rate, the symmetrical elliptical vibration locus generated by the phase difference at 90° can alternately activate multiple slip systems, and the periodic stress reversal may promote cross-slip between {110}{111} systems [27]. Additionally, the 90° phase difference results in the maximum acceleration of the tool and momentary high temperature, which in turn induces significant transient hydrostatic pressure, and promotes grain refinement in tungsten alloy materials.

6. Discussions

In UEVC process, the interaction of various vibration parameters leads to a significant increase in the strain rate in machining region. Owing to the nonlinear influence of vibration parameters on strain rate, traditional theoretical modeling methods are inadequate for quantitatively analyzing these complex influence patterns. Consequently, this study employs FEM to conduct an in-depth analysis into the relationship between vibration parameters and strain rate, revealing elucidating their respective influence laws and sensitivities. These findings provide explicit theoretical guidance for optimizing high-strain-rate processing via UEVC. Tungsten alloys exhibit pronounced sensitivity to both strain rate and temperature. Although studies based on SHPB tests have yielded critical insights into the dynamic behavior of tungsten alloys, the strain rate ranges explored therein remain substantially lower than those

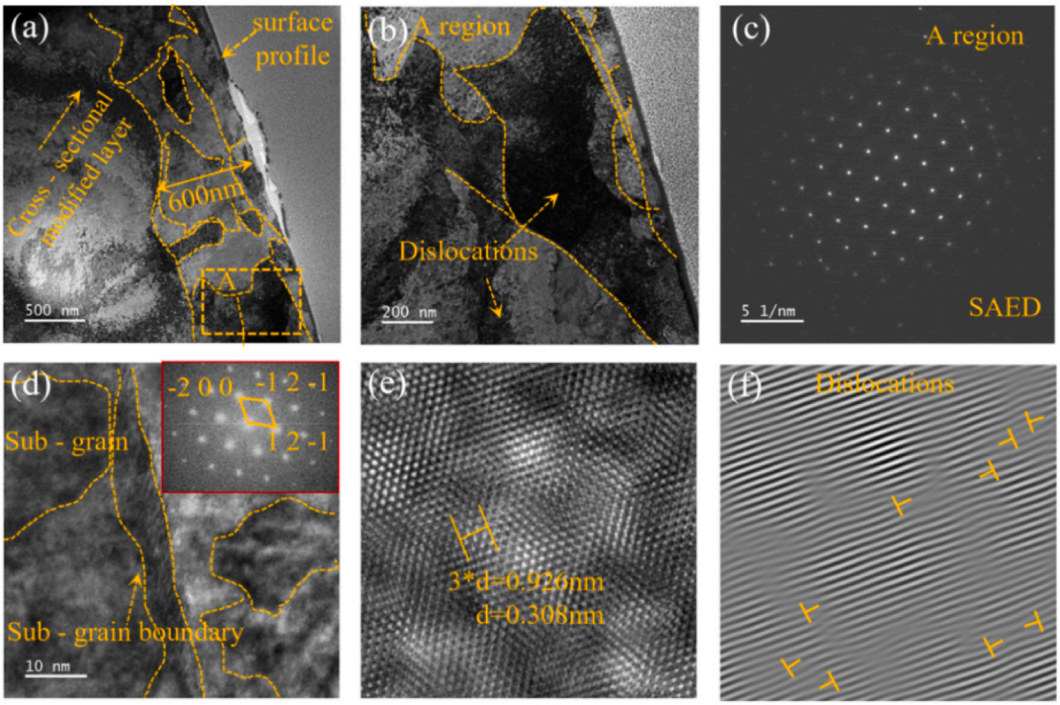

Fig. 13. Microstructural features of tungsten alloys in UEVC with 30°. (a) general view of microstructure gradient variation, (b) nanocrystalline feature of A region, (c) diffraction spots of A region, (d) grain refinement in the recrystallization layer, (e) interplanar spacing of A region, (f) inverse IFFT of A region.

encountered in UEVC. Considering that metallic materials exhibit different mechanical properties across varying strain rate regimes, this study systematically investigates cutting experiments by selecting the most sensitive phase difference as a variable in UEVC. Through detailed analysis of machined surface topography, the research reveals that tungsten alloys undergo high-stress and severe plastic deformation under high strain rates. This facilitates plastic-mode cutting, thereby significantly enhancing the machinability of tungsten alloys. This mechanistic insight further explains the pronounced enhancements observed utilizing UEVC.

The process optimization strategy based on "phase difference sensitivity" proposed in this study offers a broader phase difference regulation range (0°–180°) compared to the existing regulation of two-phase amplitude and frequency. This facilitates precision control over machined surface quality and microstructure, making it suitable for UPM of various difficult-to-machine materials. Furthermore, adjusting the phase difference through the control system can reduce economic costs by over 60 % compared to adjusting amplitude and frequency (development cost of high-performance UEVC devices). Simultaneously, precision process control can enhance tool lifespan by more than 30 %.

Tungsten alloy materials exhibit pronounced strain rate effects during dynamic loading. In UEVC, the complex periodic "tensile-compressive" stresses at high strain rates significantly enhance the dislocation nucleation rate in tungsten alloys, far exceeding the dynamic recovery rate, resulting in a rapid increase in dislocation density. This phenomenon not only leads to increased dislocation interactions and unsaturated bond formation but also reduces the yield strength of tungsten alloys, thereby improving machining quality. Furthermore, the substantial increase in surface dislocation density enhances the alloy's resistance to high-energy particle irradiation, which is crucial for extending the service life of tungsten alloys components in nuclear fusion devices [40,41].

As the phase difference increases, the strain rate in the machining region gradually rises, accompanied by significant changes in the degree of plastic deformation. These changes result in differences in the dynamic recrystallization process, increasing the thickness of the refined grain layer from 600 nm to 1300 nm. This finding provides a new research perspective: by adjusting the phase difference, it is possible to achieve precise control over strain rate and thermodynamic states during UEVC, enabling targeted modulation of the deformation mechanisms in tungsten alloys. Such control strategies not only enhance the machining performance of tungsten alloys but also hold significant potential for improving their fatigue resistance, offering new possibilities for practical engineering applications. Moreover, the method of regulating the strain rate in the cutting zone in this investigation offers significant insights and references for processing other difficult-to-machine materials. For instance, during ultrasonic vibration-assisted machining of aviation titanium alloy blades, the strategic combination of ultrasonic vibration parameters elevates the strain rate in cutting zone to 10^{-5}•s^{-1}. This triggers the adiabatic shear effect, substantially diminishing cutting forces and yielding a threefold increase in machining efficiency. Similarly, in ultrasonic vibration scribing of semiconductor ceramic substrates, modulating the phase difference and amplitude combination enables dynamic strain rate control, effectively suppressing chipping and related defects. Crucially, the development of digital twin applications, such as strain rate-surface integrity mapping databases, represents a foreseeable frontier development direction.

7. Conclusions

(1) Utilizing SHPB experiment, strain-stress curves of tungsten alloys were obtained at different temperatures. It was observed that tungsten alloys exhibits notable strain-rate sensitivity, with its mechanical properties and fracture mechanisms significantly influenced by variations in strain rate, which showed that regulating the strain rate in cutting zone is an important means to affect the material removal and surface forming.

(2) Based on the dynamic change of tool vibration speed, the strain rate calculation model of UEVC zone is established. Showing that the strain rate in cutting zone is related to the ultrasonic elliptical vibration parameters (frequency f, two-phase amplitude A_X and

A_Y, phase difference $\Delta\varphi$) and nominal cutting speed V_f, but it exhibits nonlinear change.

(3) The FE cutting simulation reveals the influence rule and sensitivity of ultrasonic elliptical vibration parameters on the strain rate in cutting zone: the increase of two-phase amplitude A_X and A_Y and phase difference $\Delta\varphi$ can significantly improve the strain rate in UEVC zone, and the phase difference is the most sensitive factor.

(4) The cutting experiment based on self-developed UEVC system independently shows that the increase of phase difference $\Delta\varphi$ gradually reduces the surface roughness, and the surface roughness of 32 nm is obtained under $\Delta\varphi$ 90°. This is because the increase of strain rate, combined with the temperature effect in cutting zone, strengthens the plastic removal mode of tungsten alloys.

(5) The change of phase difference $\Delta\varphi$ has a significant impact on the microstructure of tungsten alloys: with the increase of $\Delta\varphi$, the dislocation density increases to 3×10^{17} m^{-2} ($\Delta\varphi$=90°, 67 % higher than that of 30°), the depth of grain refinement layer increases to 1300 nm, and the grain size decreases significantly. This is because the nucleation rate of dislocation is significantly higher than the dynamic recovery rate under the strain rate of 1.8×10^5 s^{-1}, and the serious plastic deformation triggers a continuous dynamic recrystallization process, making the initial coarse grains separated into sub-grains by the dislocation wall and evolved into nanocrystalline grains under the shear stress.

The strain rate range of SHPB tests conducted in this study is lower than that in ultrasonic vibration machining, which makes the tests focus more on the qualitative study of tungsten alloy materials, and it is difficult to quantitatively analyze the material removal mechanism and the evolution law of microstructure in ultrasonic vibration machining. In the future, we plan to design an ultrasonic vibration-assisted SHPB test device to directly apply ultrasonic vibration to the workpiece to more clearly explore the evolution process of mechanical properties and microstructure of tungsten alloys and other materials at high strain rates.

Author contributions

Sen Yin: Writing original draft preparation, conceptualization, methodology, investigation, data curation, formal analysis. **Liu Menghao**: Software, methodology, investigation. **Yingjian Tian**: Supervision, validation, software, writing and editing, validation, visualization. **Fuchen Li**: Validation and software. **Gan Li:** Writing-reviewing and editing. **Renke Kang**: Writing-reviewing and editing, supervision,.

Declaration of competing interest

The authors declare that they have no known competing financial interests or personal relationships that could have appeared to influence the work reported in this paper.

Acknowledgement

The work described in this paper was partially supported the China Postdoctoral Science Foundation (2024M750796), the Key Research Projects of Higher Education Institutions in Henan Province (24A460010), the Henan Province Postdoctoral Research Project Funding (351351), Key Scientific Research Projects of Colleges and Universities in Henan Province (24A460001), Scientific and Technological Key Project in Henan Province (252102220074), the funding support from the Innovation and Technology Commission (ITC) of the Government of the Hong Kong Special Administrative Region (HKSAR), China. The authors would also like to express their sincere thanks to the financial support from the Research and Innovation Office of The Hong Kong Polytechnic University.

References

[1] Jiao Z, Kang R, Dong Z, Guo J. Microstructure characterization of W-Ni-Fe heavy alloys with optimized metallographic preparation method. Int J Refract Metals Hard Mater 2019;80:114–22. https://doi.org/10.1016/j.ijrmhm.2019.01.011.

[2] Zhang X, Qiao L, Zhang H, He W, Li Y, Wang P. Effect of 3 MeV Fe11+ ions pre-damage on blistering and deuterium retention in two tungsten grades. Nuclear Materials and Energy 2021;27. 101016/j.nme.2021.100973.

[3] Li JG, Wan YX. The experimental advanced superconducting tokamak. Engineering 2021:7 1523–1528. https://doi.org/10.1016/j.eng.2021.10.004.

[4] Fellinger J, Richou M, Ehrke G, et al. Tungsten based divertor development for wendelstein 7-X. Nuclear Materials and Energy 2023;37:101506. https://doi.org/10.1016/j.nme.2023.101506.

[5] Fan C, Katoh Y, Hu X. Impact of helium irradiation on the crystallographic orientation change in single-crystalline tungsten. Nucl Fusion 2021;61:076011. https://doi.org/10.1088/1741-4326/abff04.

[6] Haag JV, Wang J, Kruska K, Olszta MJ, Henager CH, Edwards DJ, Setyawan W, Murayama M. Investigation of interfacial strength in nacre-mimicking tungsten heavy alloys for nuclear fusion applications. Sci Rep 2023;13:575. https://doi.org/10.1038/s41598-022-26574-4.

[7] Wang Q, Jin Z, Zhao Y, Niu L, Guo J. A comparative study on tool life and wear of uncoated and coated cutting tools in turning of tungsten heavy alloys. Wear 2021;482–483:203929. https://doi.org/10.1016/j.wear.2021.203929.

[8] Li G, Kang RK, Wang H. A grinding force model and surface formation mechanism of cup wheels considering crystallographic orientation. J Mater Process Technol 2023;322:118187. https://doi.org/10.1016/j.jmatprotec.2023.118187.

[9] Wang F, Zhang XQ, Deng H. A comprehensive study on electrochemical polishing of tungsten. Appl Surf Sci 2019;475:587–97. https://doi.org/10.1016/j.apsusc.2019.01.020.

[10] Liu J, Chen G, Yu Z, Jia X, Huang J. Characterization of physical and mechanical properties of tungsten alloy surfaces for electroplasticity-assisted dry cutting machining. International Journal of Precision Engineering and Manufacturing-Green Technology 2024;11:1745–55. https://doi.org/10.1007/s40684-024-00619-7.

[11] Yin S, Wang XQ, Dong ZG, Pan YA. A cutting force prediction model for ultrasonic elliptical vibration cutting of tungsten alloys based on NSGA-II-improved BP neural network. Proc IME B J Eng Manufact 2025. https://doi.org/10.1177/09544054251325979.

[12] Li G, Liu J, Pan Y, Bao Y, Yin S, Dong Z, Kang R. Cutting chatter in ultrasonic elliptical vibration cutting and its influence on surface roughness and tool wear. Metals 2023;13:1078. https://doi.org/10.3390/met13061078.

[13] Su H, Dong Z, Bao Y, Kang R, Yin S. Formation mechanism of ductile surface in ultrasonic elliptical vibration cutting of tungsten alloys basing on cemented carbide tools. J Mater Res Technol 2025;35:5782–95. https://doi.org/10.1016/j.jmrt.2025.02.229.

[14] Pan Y, Kang R, Dong Z, Du W, Yin S, Bao Y. On-line prediction of ultrasonic elliptical vibration cutting surface roughness of tungsten heavy alloy based on deep learning. J Intell Manuf 2022;33:675–85. https://doi.org/10.1007/s10845-020-01669-9.

[15] Pan Y, Kang R, Bao Y, Pan Y, Dong Z. Study on tool wear mechanism of single-crystal diamond in ultrasonic vibration elliptical cutting of tungsten heavy alloy. Wear 2023;516:204616. https://doi.org/10.1016/j.wear.2022.204616.

[16] Yin S, Kang R, Bao Y, Yin S, Dong Z. Development and optimization of ultrasonic elliptical vibration cutting device based on single excitation. Journal of Manufacturing Science and Engineering-Transactions of the Asme 2021;143:081005. https://doi.org/10.1115/1.4049965.

[17] Yin S, Bao Y, Pan Y, Dong Z, Jin Z, Kang R. Design of ultrasonic elliptical vibration cutting system for tungsten heavy alloy. Front Mech Eng 2022;17:59. https://doi.org/10.1007/s11465-022-0715-1.

[18] Wang H, Yang GL, Su H, et al. Insight into surface formation mechanism during ultrasonic elliptical vibration cutting of tungsten alloy by scratching experiment and molecular dynamics. Tribol Int 2024;191:109088. https://doi.org/10.1016/j.triboint.2023.109088.

[19] Zhao Q, Guo X, Wang H, Yin S, Kang R, Dong Z, Bao Y. Effects of ultrasonic vibration cutting trajectories on chip formation of tungsten alloys. J Manuf Process 2023;92:147–56. https://doi.org/10.1016/j.jmapro.2023.02.053.

[20] Pan Y, Bai J, Xu Z. Theoretical and numerical studies of surface microstructural transformation in ultrasonic elliptical vibration cutting tungsten heavy alloys. Int J Adv Des Manuf Technol 2022;123:3943–53. https://doi.org/10.1007/s00170-022-10293-1.

[21] Selvam K, Mandal P, Grewal HS, Arora HS. Ultrasonic cavitation erosion - corrosion behavior of friction stir processed stainless steel. Ultrason Sonochem 2018;44:331–9. https://doi.org/10.1016/j.ultsonch.2018.02.041.

[22] Wang Z, Niu Y. Effect of ultrasonic vibration extrusion cutting on the corrosion resistance of ultra-fine grained strips. J Sci Adv Mater Devices 2023;8:100628. https://doi.org/10.1016/j.jsamd.2023.100628.

[23] Wang Z, Niu Y, Sun H, Jiao F. Preparation and mechanism of copper ultra-fine grain strip by ultrasonic vibration extrusion cutting-model, FEM and experiment. J Mater Res Technol 2023;24:4919–34. https://doi.org/10.1016/j.jmrt.2023.04.133.

[24] Liu R, Zhao W, Tian Y, Zhang J, Luo G, Shen Q. The synergetic effect of TaC particles and re alloy on microstructure and mechanical properties in tungsten

alloy. J Mater Res Technol 2024;28:4639–46. https://doi.org/10.1016/j.jmrt.2024.01.035.
[25] Zhang L, Chen X, Huang Y, Liu W, Ma Y. Microstructural characteristics and evolution mechanisms of 90W-Ni-Fe alloy under high-strain-rate deformation. Mater Sci Eng 2021;811:141070. https://doi.org/10.1016/j.msea.2021.141070.
[26] Bai J, Xu Z, Qian L. Precision-improving manufacturing produces ordered ultra-fine grained surface layer of tungsten heavy alloy through ultrasonic elliptical vibration cutting. Mater Des 2022;220:110859. https://doi.org/10.1016/j.matdes.2022.110859.
[27] Yin S, Yip WS, Dong Z, Kang R, To S. Experimental and simulation investigation of ultrasonic elliptical vibration cutting of tungsten alloys in ultra-precision machining. J Mater Res Technol 2025;34:77–89. https://doi.org/10.1016/j.jmrt.2024.12.026.
[28] Lei X, Xiang D, Peng P, Liu G, Li B, Zhao B, Gao G. Establishment of dynamic grinding force model for ultrasonic-assisted single abrasive high-speed grinding. J Mater Process Technol 2022;300:117420. https://doi.org/10.1016/j.jmatprotec.2021.117420.
[29] Yin Z, Cheng J, Dai C, Miao Q, Xu H, Sun Q, Li H, Liang Z, Li Z. Generation mechanism of the surface morphology on tilted ultrasonic elliptical vibration cutting TC4 titanium alloy. Precis Eng 2024;88:135–47. https://doi.org/10.1016/j.precisioneng.2024.01.018.
[30] Kong X, Wang E, Li S, Lin H, Zhang Z, Ju Y. Dynamic mechanical characteristics and fracture mechanism of gas-bearing coal based on SHPB experiments. Theor Appl Fract Mech 2020;105:102395. https://doi.org/10.1016/j.tafmec.2019.102395.
[31] Wang Z, Ding H, Xiao Z, Yang C, Xiang C. Experimental investigation on the mechanical properties and strain rate sensitivity of mg–al–ca–mn alloy under various strain rates. Mater Sci Eng 2021;826:141997. https://doi.org/10.1016/j.msea.2021.141997.
[32] Merle B, Higgins WH, Pharr GM. Critical issues in conducting constant strain rate nanoindentation tests at higher strain rates. J Mater Res 2019;34:3495–503. https://doi.org/10.1557/jmr.2019.292.
[33] Dewhurst P. On the non-uniqueness of the machining process. Proceedings of the Royal Society A Mathematical Physical & Engineering Sciences 1972;12:105–20. https://doi.org/10.1098/rspa.1978.0087.
[34] Rubenstein C. The influence of strain rate in orthogonal cutting. Int J Mach Tool Des Res 1972;12:105–20. https://doi.org/10.1016/0020-7357(72)90026-1.
[35] Wang L, Yue C, Liu X, Li M, Xu Y, Liang SY. Conventional and micro scale finite element modeling for metal cutting process: a review. Chin J Aeronaut 2024;37:199–232. https://doi.org/10.1016/j.cja.23.03.004.
[36] Sahoo P, Patra K, Singh VK, Mittal RK, Singh RK. Modeling dynamic stability and cutting forces in micro milling of Ti6Al4V using intermittent oblique cutting finite element method simulation-based force coefficients. J Manuf Sci Eng 2020;142:091005. https://doi.org/10.1115/1.4047432.
[37] Sun J, Li P, Wang K, Zhang R, Chen G, Zhao M, Dai M, Zhang Y, Shao D. Research on ultrasonic elliptical vibration-assisted cutting system based on double excitation. Int J Adv Des Manuf Technol 2024;133:1379–91. https://doi.org/10.1007/s00170-024-13862-8.
[38] Yao G, Zhang D, Geng D, Wang L. Novel ultrasonic vibration-assisted electrosurgical cutting system for minimizing tissue adhesion and thermal injury. Mater Des 2021;201:109528. https://doi.org/10.1016/j.matdes.2021.109528.
[39] Gao P, Xu Z, Zhao X, Li S, Wang M, Jing L, Zan T. Cutting behaviors of cortical bone ultrasonic vibration-assisted cutting immersed in physiological saline. Ultrason Sonochem 2024;111:107135. https://doi.org/10.1016/j.ultsonch.2024.107135.
[40] Castin N, Bonny G, Bakaev A, Ortiz CJ, Sand AE, Terentyev D. Object kinetic monte carlo model for neutron and ion irradiation in tungsten: impact of transmutation and carbon impurities. J Nucl Mater 2018;500:15–25. https://doi.org/10.1016/j.jnucmat.2017.12.014.
[41] Lin J-S, Luo L-M, Xu Q, Zan X, Zhu X-Y, Wu Y-C. Microstructure and deuterium retention after ion irradiation of W–Lu2O3 composites. J Nucl Mater 2017;490:272–8. https://doi.org/10.1016/j.jnucmat.2017.04.042.